Smart Structures and Systems, *Vol. 36, No. 3 (2025) 179-194*
https://doi.org/10.12989/sss.2025.36.3.179

Hybrid neural network techniques for friction capacity prediction in concrete pile foundations

Huanyang Xiao [1a], Mesut Gör [2b], Junlong Shi [3c], Mohammad Hannan [4d], Hossein Moayedi*[5,6] and Gamil M.S. Abdullah [7e]

[1] *Zhejiang Geology and Mineral Technology Co., China LTD., China*
[2] *Department of Civil Engineering, Faculty of Engineering, Firat University, Elazığ, Turkey*
[3] *11th Geology Team of Zhejiang Province, China*
[4] *Former Student of Applied Mathematics, Shiraz University of Technology, Shiraz, Iran*
[5] *Institute of Research and Development, Duy Tan University, Da Nang, Vietnam*
[6] *School of Engineering & Technology, Duy Tan University, Da Nang, Vietnam*
[7] *Department of Civil Engineering, College of Engineering, Najran University, Najran, Saudi Arabia*

(*Received December 28, 2023, Revised August 21, 2025, Accepted October 15, 2025*)

Abstract. The advancement of novel data mining and optimization algorithms has significantly enhanced traditional engineering structural analysis models, particularly those based on swarm intelligence. This study delves into refining the neural assessment of shaft friction capacity in driven pile systems by exploring the social behavior of four hybridized algorithms: Wind-Driven Optimization (WDO), Spotted Hyena Optimization (SHO), Grasshopper Optimization Algorithm (GOA), and Moth–Flame Optimization (MFO). Four crucial influencing variables — pile length (m), diameter (cm), effective vertical stress (Sv), and undrained shear strength (Su) — are considered in constructing the requisite dataset. After applying optimized structures, each ensemble undergoes a sensitivity analysis based on its individual swarm size. The predictive precision of the models is compared using the results of two sensitivity analyses. Neural network simulations exhibit improved results with an increased number of neurons in a single hidden layer. The root mean square errors (RMSEs) for the training and test datasets, employing Multilayer Perceptron (MLP)-based solutions, are (0.05241, 0.32861, 0.06155, and 0.03874) and (0.04334, 0.18155, 0.05382, and 0.03626), respectively. In the training and testing datasets for proposed predictive models using WDO, SHO, GOA, and MFO, R^2 values of (0.996, 0.853, 0.992, and 0.997) and (0.985, 0.732, 0.997, and 0.997) were found, respectively. Notably, MFO outperforms its counterparts when integrated with MLP for predicting engineering solutions.

Keywords: driven piles; hybrid; neural network; optimization; shaft friction capacity

1. Introduction

Heavy loads can be safely transferred to the bedrock or competent soils beneath using structural members such as pile foundations (Sun *et al*. 2017, Wang *et al*. 2024, Zheng and Baudet 2025). When working with cohesive soils, concrete-driven piles can be installed with impact hammers (Li *et al*. 2017). Various factors influenced the final bearing capacity of these piles. Pile types can be divided into subcategories based on their installation method. Driven piles are made of various materials, including precast concrete, steel, and wood. This type of piling is typically built by hammering a pile into place using the force of falling. The fractional elastoplastic constitutive model for soils based on a novel 3D fractional plastic flow rule can enhance the accuracy of structural design by more realistically capturing the time-dependent and nonlinear stress–strain behavior of soils under complex loading conditions (Lu *et al*. 2019). Friction between the soil and the pile structure, or skin friction, affects a pile's load-bearing capacity and can extend to the pile toe. Because the soil–pile interaction is so complex, no method has yet accurately predicted the friction capacity of piles subjected to axial compressive load (Alkroosh and Nikraz 2012, Cheng and Liu 2012, Franza *et al*. 2021). Geotechnical engineers must, therefore, predict the friction capacity of piles. In the literature, several methods exist for determining frictional capacity, including effective stress-based approaches, a total stress-based model, and a better method that combines the best of each (Baker *et al*. 1984, Coduto *et al*. 2001, Randolph 2003). Numerous factors complicate the development of an accurate, theoretical, and statistical model for piles, including their nonlinear interactions with soil, their loading rate, and the impact of ground-level changes on pile performance over time (Tomlinson and Woodward 2007, Chiou *et al*. 2017).

It is rare to see naturally occurring soils gathered in uniform soil layers (Zhao *et al*. 2023). The ultimate

*Corresponding author, Ph.D.,
E-mail: hosseinmoayedi@duytan.edu.vn
[a] B.Sc., E-mail: 545769012@qq.com
[b] Ph.D., E-mail: mgor@firat.edu.tr
[c] B.Sc., E-mail: 591329253@qq.com
[d] M.Sc., E-mail: mohammad.hannan.MH@gmail.com
[e] Ph.D., E-mail: gmabdullah@nu.edu.sa

ISSN: 1738-1584 (Print), 1738-1991 (Online)

carrying capacity of multilayer soil is often not evaluated in the same way as that of a single layer, since the stability and stiffness of each layer differ (Jang 2022). Theories of soil carrying capacity with multiple layers have received significant attention from academics. In this sense, two scenarios can be classified as inhomogeneous sand layers: Two situations exist: (1) thicker soil layered over a thinner layer of sand, and (2) thinner soil layered over a layer of dense soil (Mosallanezhad and Moayedi 2017). Calculation techniques often take into account the following: By applying Eqs. (1)-(2) found in references (Bowles 1988), the maximum q_{ult} or bearing capacity may be designed.

$$q_{\text{ult-Terzaghi(1943)}} = c'N_c + qN_q + \frac{1}{2}\gamma BN_\gamma \quad (1)$$

$$q_{\text{ult-Hasen(1970)}} = c'N_c d_c S_c + q'N_q d_q S_q + \frac{1}{2}\gamma BN_\gamma d_\gamma S_\gamma \quad (2)$$

The parameters of the carrying capacity based on the internal friction angle (φ), the overburden pressure (q), the soil unit weight (γ), the cohesiveness (c'), and the footing width (B) are denoted by the symbols N_c, N_q, and N_γ in the relationships mentioned above.

The predictive challenge of estimating shaft friction capacity in driven piles had been recognized as a highly nonlinear geotechnical problem influenced by multiple interdependent factors. Parameters such as pile length, pile diameter, effective vertical stress, and undrained shear strength had played critical roles. Yet their interactions often exhibited complex behaviors that traditional regression-based or empirical models did not capture with sufficient precision. The reliance of conventional approaches on oversimplified assumptions regarding soil–structure interaction had further restricted their generalizability across diverse geotechnical conditions. In this sense, swarm intelligence algorithms have offered a promising solution to these limitations because of their inherent capacity to escape local optima, maintain a balance between global exploration and local exploitation, and adapt efficiently to multidimensional data environments. These characteristics had made them particularly suitable for problems where nonlinear dependencies and heterogeneous datasets had dominated, as is frequently the case in pile capacity prediction. By integrating swarm intelligence with multilayer perceptron neural networks, it has been possible to refine model training and improve predictive accuracy through more effective parameter optimization. Samui *et al*. investigated the friction capacity of driven piles using a well-known support vector machine classification method (Samui 2008). Wang *et al*. (2025) experimentally evaluate the axial load-bearing behavior of grout-lifted compressible concrete-filled steel tube composite columns, revealing that their yielding structure effectively controls deformation and enhances ultimate load-bearing capacity by 13–24% compared to non-compressible columns, and propose a theoretical formula for their ultimate bearing capacity. Yin *et al*. (2023) developed and validated a theoretical model to predict the deformation of tunnels underlying foundation pit excavations, showing that tunnel uplift follows an "n"-shaped profile and is strongly influenced by foundation soil stiffness and tunnel burial depth, with theoretical predictions closely matching measured results. Hu *et al*. (2025) presented a reliable prediction method for ground settlement in rectangular tunnel construction, validated through numerical models and field cases, demonstrating strong agreement with measured data and improved accuracy compared with existing approaches. Several studies contributed to understanding elastic–plastic interactions by offering advanced elastoplastic modeling frameworks that capture material nonlinearity and environmental influences, essential for accurately predicting structural behavior under complex loading conditions (Lu *et al*. 2023, Lin *et al*. 2024). Recent studies have demonstrated the effectiveness of advanced modeling and diagnostic approaches in assessing and enhancing reinforced concrete (RC) structures. For instance, deep learning frameworks have been utilized for subsurface defect quantification using array ultrasound and dual-scale neural networks or plastic deformation prediction (Niu *et al*. 2024, Cao and Wang 2025, Shu *et al*. 2025), while the influence of elevated temperatures on punching shear behavior in RC slab–column connections has been experimentally explored (Weng *et al*. 2025). Moreover, rehabilitation strategies for corroded RC columns under combined loadings (Huang *et al*. 2020) and novel Voronoi-based RBSM modeling techniques for RC structures Gong and Li (2024) and Zhang *et al*. (2024b) have further advanced predictive and analytical capabilities in structural engineering. Similarly, Prakash *et al*. (2025) and Song *et al*. (2025) emphasized the use of artificial intelligence for structural health monitoring or crack detection, respectively. Prediction of material shear parameters and in situ creep are also examples of the use of similar intelligent techniques (Huang *et al*. 2023, Li *et al*. 2025, Yang *et al*. 2025).

Machine learning was later used to determine pile bearing capacity, which remains one of the most accurate methods available. Tian and Wei (2009) accurately predicted skin friction in driven piles. An extensometer instrument placed at each end of the pile can be used to measure stress differences during testing. Samui evaluated the same design parameter using a more advanced technique, MARS (multivariate adaptive regression splines). Alkroosh and Nikraz (2012) proposed a novel artificial intelligence computing method to approximate the axial bearing capacity of driven piles in clayey soil. Samui *et al*. developed a model to determine the ultimate bearing capacity of driven pilings installed in the sand (Samui 2012). According to the findings, MARS is an effective geotechnical engineering tool that can be used well (Zhang 2020). Advanced numerical methods, such as the hyper dual step derivative–based return-mapping algorithm and hybrid quantum genetic optimization techniques, can be leveraged to improve soil–structure interaction modeling and to optimize pile bearing capacity and structural design under complex loading conditions (Zhou *et al*. 2023, Xu *et al*. 2025). Similar smart techniques are suggested for Multi-mode fatigue life prediction (Hao *et al*. 2025), mechanical properties of materials under compression (Ma *et al*. 2025),

Inter-storey isolation (Zhang *et al*. 2024a), and thermal performance and pore structure of cement–based composites (Liu *et al*. 2025). Huang *et al*. (2022) proposed two novel steel–concrete composite frame beams, SHSFB and SPSFB, that exhibit steel-like behavior, high seismic performance, ease of construction, and material efficiency, as confirmed by cyclic loading tests that showed excellent ductility, energy dissipation, and optimized design parameters.

Moayedi and Hayati (2019) present a series of design solution charts for driving piles in cohesive soils. Artificial intelligence-based techniques were used to determine the ultimate bearing capacity of the driven piles. Statistical indices were used to select the best model. The most effective predictive networks generated and displayed a series of design solution graphs.

In recent years, the prediction of shaft friction capacity in pile foundations has increasingly relied on data-driven modeling approaches, given the complex, nonlinear interactions among pile geometry, soil properties, and stress conditions. Traditional empirical and analytical models often fall short in capturing these intricacies, especially under diverse geotechnical conditions. In this context, swarm intelligence algorithms have emerged as powerful tools for solving nonlinear optimization problems in engineering. Inspired by collective behaviors in nature, algorithms such as Wind-Driven Optimization (WDO), Spotted Hyena Optimization (SHO), Grasshopper Optimization Algorithm (GOA), and Moth–Flame Optimization (MFO) offer robust global search capabilities and adaptability in high-dimensional spaces. These features make them particularly well-suited for enhancing neural network training and avoiding local minima—limitations often encountered in gradient-based optimization. Unlike conventional machine learning models, which may suffer from premature convergence or overfitting, hybridizing swarm algorithms with Multilayer Perceptron (MLP) networks enables the proposed models to achieve superior predictive accuracy and generalization. This study investigates the integration of four such hybrid models for estimating shaft friction capacity. It demonstrates their ability to outperform traditional approaches, thereby providing a more reliable decision-support framework for geotechnical design. Despite advancements in empirical and numerical modeling techniques, existing methods for predicting shaft friction capacity in driven pile systems still face notable limitations. Empirical formulas, while widely used in design codes, often rely on oversimplified assumptions and are highly sensitive to local soil conditions, leading to inconsistencies in prediction accuracy. Conventional machine learning models, although more flexible, often rely on local optimization and may struggle with nonlinear, high-dimensional datasets, leading to poor generalization or convergence to suboptimal solutions. This research addresses these gaps by proposing a hybrid modeling approach that integrates swarm intelligence algorithms with Multilayer Perceptron (MLP) neural networks. By leveraging the global search strengths of swarm algorithms and the nonlinear mapping capabilities of MLP, the proposed models offer improved prediction accuracy, enhanced convergence behavior, and greater

Table 1 The variation of the data used in this study

Pile length (m)	Pile diameter (cm)	Vertical effective stress (kPa)	Undrained shear strength (kPa)	ISFC (kPa)
14.1	15	96	26	27
11.7	20	54	23	14
17.5	14.3	87	23	26
15.9	15	49	17	12
8.1	13.5	37	13	11
7.7	16.5	32	15	9
12	15.5	39	12	10
10.2	22	19	15	8
24.2	15	146	19	29
17.1	15.9	109	57	24
12.7	23.2	38	19	17
5.5	30.5	44	30	38
19.2	61	142	31	30.7
15.2	35.6	448	104	109.2
12.2	35.6	718	162	162
96	61	354	80	44
73.8	61	273	67	47.6
30.5	32.5	153	45	29.3
45.7	32.5	148	52	21.8
13.7	32.5	112	45	42.3
29	33	105	39	39.8
12.2	16.8	33	16	9.9
14	35.1	59	30	23.4
39.6	27.4	297	165	80.9
25.9	32.5	99	61	34.2
13.1	27.4	80	110	53.9
20.1	61	105	208	91.5
13.7	32.5	112	137	64.4
18.3	76.2	115	335	154.1
4.6	16.9	43	120.5	84.6
33.6	32.5	121.4	35.4	30.4
33.6	32.5	108	48.8	27.1
3.5	51	102.8	24.4	23.5
8	13.5	27	9	9
11.6	17.5	57	27	18
9.6	19.2	42	15	13
36.9	30.6	149	28.2	30.5
66.4	32.5	223	60	31.2
11.6	11.4	44	21	13.4
22.9	32.5	91	52	27
13.8	19	27	21	13
25.3	27.4	244	185	88.8
18.3	32.5	51	33	32
48.2	61	152	64	37.8
32	27.4	141	115	59.8

Table 1 Continued

Pile length (m)	Pile diameter (cm)	Vertical effective stress (kPa)	Undrained shear strength (kPa)	ISFC (kPa)
13.4	27	81	22	20
24.2	15	147	19	30
15.5	17.5	80	72	35
20.3	32.5	158.2	112.8	53
9.1	45	54	144	73.4
10	17	82	36	28
14.3	26	89	22	22
10	13.5	33	10	12
13	15	102	15	26
43.9	30.5	162	38	30
5.5	16.9	51.6	129.5	76.7
9.4	29.3	52	29	18
14.6	16	67	29	16
30.5	61	91	52	30.7
14.9	52.8	66	53	27.6
22.6	76.7	651	170	92.1
21.6	45.7	147	31	28.8
22.5	47	60	45	23
12.8	32.5	110	96	54.7
16.8	61	87	100	55

robustness in capturing complex soil-pile interactions. This work contributes to the field by advancing predictive modeling techniques and systematically comparing the performance of four distinct hybrid algorithms (WDO-MLP, SHO-MLP, GOA-MLP, and MFO-MLP), thereby identifying optimal configurations for practical geotechnical applications.

2. Established data

Sixty-five in-situ tests were conducted to generate the datasets. The data used are tabulated in Table 1. Data from Goh (1996) were used to develop optimal structures (e.g., GOA, WDO, SHO, and MFO) using MLP models. Additionally, pile load test results are collected, along with data on nearby soil properties. As a result, the training and testing sets are built based on extensive in-situ investigations. Both models are trained on a dataset of 52 field experiments and then tested on 11 tests. Both the input data (e.g., pile length (m) and diameter (cm)) and the output data (e.g., the friction capacity of installed shafts) are subject to change, as shown in Fig. 1.

3. Methodology

This study detailed the MLP architecture for reproducibility. To simplify the network output, only a single hidden layer was used. The number of neurons was set through iterative experiments. The final configuration minimized error and maintained computational feasibility. Split validation was used during training to assess generalization and reduce overfitting. Note that split validation is a method to evaluate a machine learning model's performance. The dataset is divided into two parts: a training set and a test set. Typically, 70-80% of the data is used for training, and 20-30% for testing. The model is trained on the training set and then tested on the test set to evaluate its performance on unseen data. This helps assess if the model generalizes well and avoids overfitting, where it performs well only on the training data. The split is usually random but can be stratified to maintain class balance. At the end of each step, the performance improvements were held on unseen data, not just the training set. During the hybrid modeling evaluation, sensitivity analyses were conducted to assess the influence of swarm size on model performance. The number of agents in each optimization algorithm was varied systematically within a defined range, and the resulting predictions were assessed using standard performance metrics. This process had enabled the identification of swarm sizes that had provided a balance between convergence stability and computational efficiency. By examining variations in error and predictive consistency across different swarm sizes, the analysis established a clearer understanding of the role of swarm population in shaping the accuracy of the hybrid models. In addition, comprehensive data preprocessing was undertaken before model training. All input variables had been normalized to a common scale to eliminate disparities caused by differing units and magnitudes, thereby facilitating stable learning by the neural network. Outlier values were detected and handled carefully to prevent distortion of predictive patterns, and dataset completeness was confirmed through systematic checks for missing entries. When necessary, corrective measures had been applied to preserve the integrity and representativeness of the data. In addition, comprehensive data preprocessing was done before model training. All input variables were normalized to a common scale to remove differences in units and magnitudes, which helped the neural network learn more stably. Outlier values were found and handled carefully to avoid distorting predictive patterns.

● Artificial Neural Network

The architecture of the ANN model is depicted in Fig. 2. The diagram illustrates the structure of an MLP model developed to predict the shaft friction capacity of piles. Four input variables—pile length, pile diameter, vertical effective stress, and undrained shear strength—are introduced into the network. These inputs are processed through hidden layers, where activation functions f_1 and f_2 transform weighted combinations of the variables. The hidden nodes are connected to the output layer through adjustable weight parameters (β_1 and β_H), enabling the network to learn nonlinear relationships. The final output provides the predicted friction capacity in kilopascals (kPa), capturing the combined influence of geotechnical parameters.

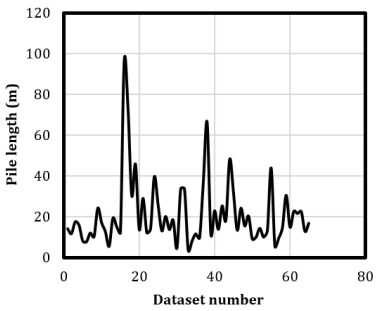

(a) Pile length (m)

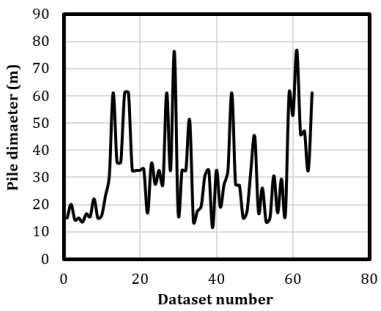

(b) Pile diameter (m)

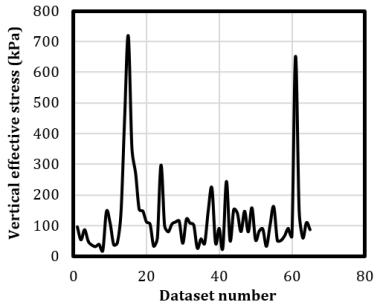

(c) Vertical effective stress (kPa)

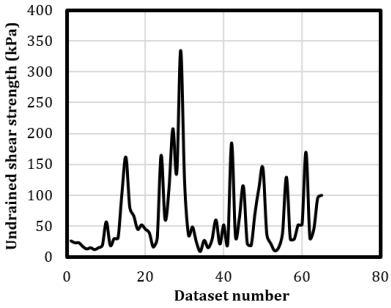

(d) Undrained shear strength (kPa)

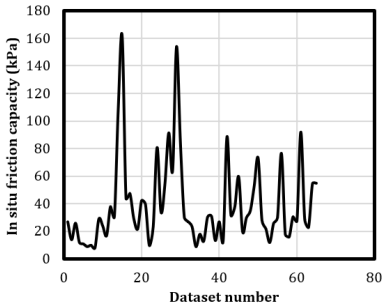

(e) In situ friction capacity (kPa)

Fig. 1 Input and output parameters

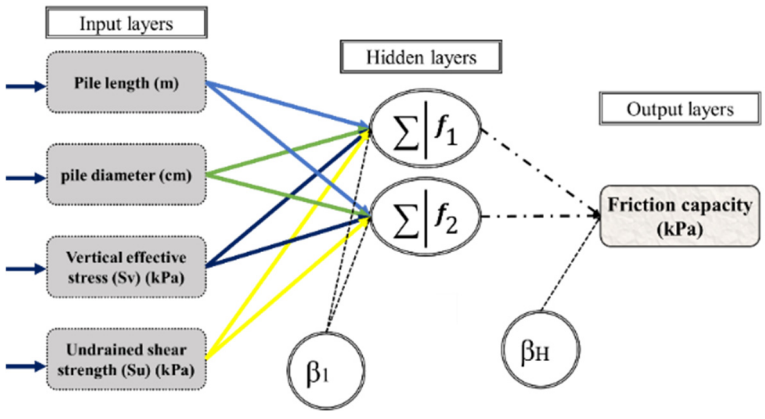

Fig. 2 A multilayer perceptron structure can be used to predict the friction capacity of a shaft

● Hybrid model development

The input parameters in Fig. 3 were used to forecast the experiment's outcome. Metaheuristic algorithms are used in conjunction with MLP. In these algorithmic combinations, the Levenberg-Marquardt (LM) training procedure is replaced by optimization methods. The following steps must be followed succinctly:

a) Choosing the optimal MLP model structure for use.
b) Defining and solving the problem function using the WDO-MLP, SHO-MLP, GAO-MLP, and MFO-MLP.
c) Correctly specify variables such as the algorithm's population size, the number of iterations, and the

objective function.

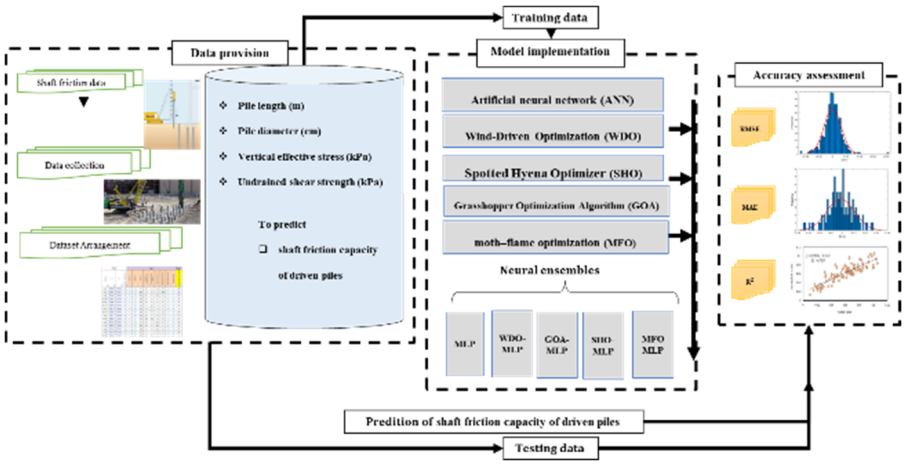

Fig. 3 Flowchart with input parameters for shaft friction capacity prediction

objective function.

d) Adjusting the MLP's weights and biases can help reduce its error.
e) The optimal solution is preserved when a stop requirement is met.

The major objective of this study is to determine the MSE. It assesses the quality of the solution created in each iteration. Eq. (3) can be used to compute RMSE.

$$MSE = \frac{1}{U}\sum_{i=1}^{U} |S_{i_{observed}} - S_{i_{predicted}}| \quad (3)$$

$S_{i_{observed}}$, and $S_{i_{predicted}}$ indicate the actual and expected GDP numbers, respectively. U also denotes the number of samples. Convergence curves are generated by plotting the calculated RMSEs and MAEs and comparing them to determine how the models improve with additional iterations. The curves for the eleven population sizes analyzed are depicted in Fig. 6: 50, 100, 150, 200, 250, 300, 350, 400, 450, and 500. There is no correlation between the difficulty of the approaches utilized in this study and the difficulty of resolving the problem.

The selection of WDO, SHO, GOA, and MFO was based on their diverse underlying heuristics, global search capabilities, and successful applications in complex engineering problems. These algorithms represent different categories of swarm and nature-inspired intelligence: WDO simulates atmospheric motion dynamics; SHO mimics cooperative hunting strategies; GOA is inspired by swarm behavior and interaction forces; and MFO models the navigational patterns of moths around flames. Compared to conventional metaheuristics such as PSO and GA, the selected algorithms offer a better exploration-exploitation balance and greater adaptability to nonlinear functions, making them well-suited for modeling complex geotechnical behaviors, such as pile-soil interaction. Moreover, these algorithms have demonstrated superior convergence properties in prior structural and geotechnical optimization tasks. A comparative analysis of their computational performance, convergence speed, and prediction accuracy has been conducted in this study, further justifying their use over more traditional methods. The inclusion of this variety also provides a broader benchmarking base to identify the most effective hybrid intelligence model for shaft friction capacity prediction.

● Wind-Driven Optimization

The metaheuristic technique WDO was developed by Bayraktar *et al.* (2010). Based on the movement of air parcels, the algorithm is constructed. To complete this task, four forces are at work: the gravitational force (FG), the pressure-gradient force (FPG), the Coriolis force (FC), and the frictional force (FF). Air parcels are assumed to have no dimensions and weight to simplify calculations. When P and δV are the pressure gradient and air volume, respectively, the force due to the pressure gradient is expressed in Eq. (4). FPG's air movement is countered by FF (Eq. (5)). FG (Eq. (6)) is in charge of getting parcels to the Earth's core. FC can be blamed for air parcel motion deflections (Eq. (7)).

$$\overrightarrow{F_{PG}} = -\nabla P.\delta V \quad (4)$$

$$\overrightarrow{F_F} = -\rho\,\alpha\,\vec{u}\,, \quad (5)$$

$$\overrightarrow{F_G} = \rho.\delta V.\vec{g}, \quad (6)$$

$$\overrightarrow{F_C} = -2\theta \times \vec{u}\,, \quad (7)$$

where g is assigned to the gravitational constant, ρ denotes the density of a short air parcel, $\vec{u}$ is the velocity vector of wind, α is a frictional coefficient, and θ is the Earth's rotation.

The ideal gas equation takes into account the previously mentioned forces, and the following is the result (Derick *et al.* 2017)

$$\overrightarrow{\nabla u} = g + \left(-\nabla P.\frac{RT}{P_{cur}}\right) + (-\alpha\vec{u}) + \left(\frac{-2\theta \times \vec{u}RT}{P_{cur}}\right) \quad (8)$$

Because air velocity is proportional to pressure,

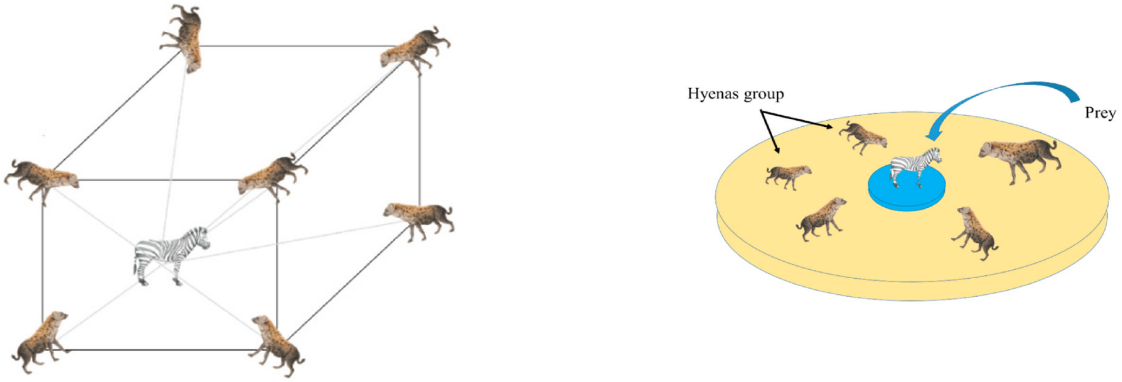

(a) (b)

Fig. 4 Hunting process carried out in the spotted hyena optimizer (SHO) algorithm: (a) position vectors and the possible next locations of the members; and (b) attacking the prey.

an increase in pressure results in a change in velocity. As a result, we've had to make a change to Eq. (8). The parcels are now sorted in descending order of the pressure applied to them. The following equations can be used to update velocity and position, with i denoting the rank

$$\overrightarrow{U_{new}} = (1-\alpha)\vec{u}_{cur} - gx_{cur} + \left(\left|1-\frac{1}{i}\right|.(x_{opt}-x_{cur})RT\right) + \left(\frac{C.\vec{U}_{otherdirection}}{i}\right) \quad (9)$$

$$\overrightarrow{X_{new}} = \overrightarrow{X_{old}} + \overrightarrow{U_{new}} \quad (10)$$

Where $\vec{u}_{cur}$ and $\overrightarrow{u_{new}}$ are assigned to the velocity of the current and coming iterations, x is the air parcel position, and x_{opt} and x_{cur} are the optimal and current positions. Meanwhile, $\vec{U}_{otherdirection}$ is equal to $\overrightarrow{F_C}$ and $C = -2RT$.

The updating procedure is complete when the predetermined objective function (OF) or number of repetitions is reached. The air parcel with the lowest OF is selected, and the associated parameters are applied. Additional information is available from previous studies (Bayraktar *et al*. 2010).

● Spotted Hyena Optimizer (SHO)

The SHO is a novel optimization technique inspired by spotted hyena hunting behavior. Spotted hyenas have been observed living and hunting in packs. This algorithm includes stages for predator hunting, prey circling, and prey attack (Fig. 4). Because the search space is unknown in advance, the most promising candidate solution is viewed as prey or an objective near the optimum during this process (Dhiman and Kumar 2018). To locate the prey, other searchers form a group of friends and travel to the elite agent's location, which is presumed to contain information about the prey's location. Previous studies have extensively described SHO (Kaur *et al*. 2018, Jia *et al*. 2019, Luo *et al*. 2019).

● Grasshopper Optimization Algorithm

Probably the most well-known fact about grasshoppers is that they are plant-eating insects that can be found alone or in groups. Saremi *et al*. (2017) developed the GOA based on grasshopper herding behavior. When natural algorithms such as the GOA search for food sources, they divide their search into two major stages: exploration and harvesting. Grasshopper behavior is depicted in Fig. 5. During implementation, several search agents fly over the search area. This is because the abrupt movement of one phase fuels these relationships. Eq. (11) illustrates swarming behavior by using X_i as the *i*th insect's position.

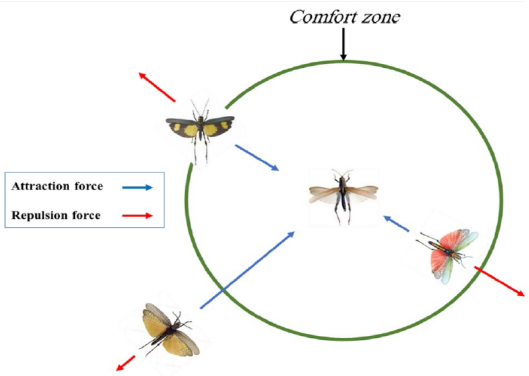

Fig. 5 The GOA method's basic corrective patterns

$$X_i = r_1 S_i + r_2 G_i + r_3 A_i \quad (11)$$

in which S_i denotes the social relationship, G_i symbolizes the gravitational force, and A_i is the wind advection. Also, r_1, r_2, and r_3 are random values ranging from 0 to 1. More mathematical details about the algorithm can be found in Aljarah *et al*. (2018), Mirjalili *et al*. (2018).

● Moth–flame optimization

Moths use a technique called transverse orientation to navigate at night when the moonlight is at its weakest. To fly, a moth must maintain a constant angle with the moon (as the light source) (Mirjalili 2015). This is an excellent method for traveling long distances in a straight line. This movement affected the algorithm described in the following section. Moths and flames serve as the primary building blocks of the algorithm. Among the possible solutions are

molecules such as moths, whose spatial positions determine the problem. When it comes to flight, moths can fly in a variety of spatial configurations, including one-, two-, three-, and even multidimensional. Due to the population-based nature of the MFO algorithm, the n moths act as search agents in the problem space. In terms of moths, the n-flame positions are the best thus far. Each month, a flag is circled in search of a better solution (flame). Alternatively, d-dimensional data points can be viewed as flames. The logarithmic spiral described by the equation is used to track the location of a moth around a particular flame (Gaston *et al*. 2013).

$$S(M_i, F_j) = D_i \,.\, e^{bt} \,.\, \cos(2\pi t) + F_j \tag{12}$$

Where D_i means the Euclidean distance of the i^{th} moth for the j^{th} flame, b is a constant for defining the shape of the logarithmic spiral, M_i denotes the i^{th} moth, F_j is the j^{th} flame and t is a random number in $[-1, 1]$.

The next month's location is determined by comparison to a flame. The value of t indicates the moth's next position in the spiral equation. To emphasize exploitability, it is assumed that random numbers are uniformly distributed over [r, 1] and [r, 2], where r decreases linearly from -1 to -2. Moths improve their ability to exploit their flames as the number of iterations increases. Each moth can update its location by utilizing only one of the flames, increasing the likelihood of a global solution. The flames are sorted by fitness after each iteration, and the list of flames is updated. They are then recalculated in relation to the fire. The number of flames to follow decreases as the number of iterations increases in Eq. (13) (Frank *et al*. 2006). MFO is depicted in the form of an algorithm (1).

$$N_{flames} = round\left(N - l \,.\, \frac{N-1}{T}\right) \tag{13}$$

Where l is the current iteration number, N is the maximum number of flames, and T indicates the maximum number of iterations.

input : n number of moths or search agents,
N maximum number of flames,
T number of iterations.
output: f_{best} optimal flame position,
$f(f_{best})$ fitness value for f_{best}.

1) Initialize a population of n flames positions randomly in the search space.
2) **while** *Stopping criteria not met* **do**
  Update the number of flames to be used N_{flames} according to equation 2.
  Calculate the fitness of all the n moths.
  if *first iteration* **then**
    Sort the moths from best to worst according to their fitness and place the result in flame matrix.
  else
    Merge the population of past moths and flames. Sort the merged population from best to worst. Select the best N positions from the sorted merged population as the flames.
  end
  Calculate the convergence constant r.
  foreach $Moth_i$ *with* $i \leq n$ **do**
    Calculate t as $t = (r-1) * rand + 1$. With $rand$ a random number drawn from uniform distribution in the range [0, 1].
    if $i \leq N$ **then**
      Update $Moth_i$ position according to $Flame_i$ using equation 1.
    else
      Update $Moth_i$ position according to $Flame_{N_{flames}}$ using equation 1.
    end
  end
  end

Algorithm 1: Moth-flame optimization (MFO) algorithm

4. Results and discussion

The friction capacity of the driven pile shaft will be predicted in this study by utilizing four techniques. We estimated friction capacity using WDO, SHO, GOA, and MFO. The dataset was randomly split into training and test sets at 70:30. The 70:30 train–test split was adopted because it is a widely accepted practice in predictive modeling, providing sufficient training data while retaining an adequate test set for independent validation. To further address concerns about robustness, k-fold cross-validation was also implemented during model development. This approach ensured that the results were not dependent on a single arbitrary data partition and that the model's performance was consistently validated across multiple folds. The inclusion of cross-validation thus strengthened the reliability of the reported outcomes. The RMSE and the determination coefficient R^2. Eqs. (14) and (15) define R^2 and RMSE, respectively.

$$R^2 = 1 - \frac{\sum_{i=1}^{N}(Y_{i\,predicted} - Y_{i\,observed})^2}{\sum_{i=1}^{N}(Y_{i\,observed} - \bar{Y}_{i\,observed})^2} \tag{14}$$

$$RMSE = \sqrt{\frac{1}{N}\sum_{i=1}^{N}\left[(Y_{i\,observed} - Y_{i\,predicted})\right]^2} \tag{15}$$

Where $Y_{i\,predicted}$ and $Y_{i\,observed}$ represent the predicted and actual f_s, and the number of instances is shown by N. Also, $\underline{Y}_{i\,observed}$ denotes the average of the actual f_s.

- The hybrid model predicting friction capacity

Under varying population sizes, illustrating how swarm size had influenced the MSE across iterations. Fig. 6(a) shows the performance of WDO-MLP, where error values had steadily decreased with iterations, and smaller swarm sizes (e.g., 50 and 100) had converged faster. In contrast, larger populations demonstrated slower but more stable reductions. Fig. 6(b) demonstrates the SHO-MLP results, which showed minimal variation across population sizes, indicating limited sensitivity to swarm size and comparatively weaker improvement in error reduction. Fig. 6(c) depicts the GOA-MLP behavior, where convergence patterns had been highly irregular, with several swarm sizes exhibiting unstable performance before eventually achieving lower MSE values at later stages. Fig. 6(d) highlights the MFO-MLP outcomes, where population sizes between 100 and 250 had yielded the most consistent and rapid convergence, outperforming larger swarm sizes that converged more slowly. The overall comparison had indicated that swarm size optimization was a critical factor influencing model accuracy and stability. While WDO-MLP and MFO-MLP showed substantial improvements with appropriate population sizes, SHO-MLP underperformed

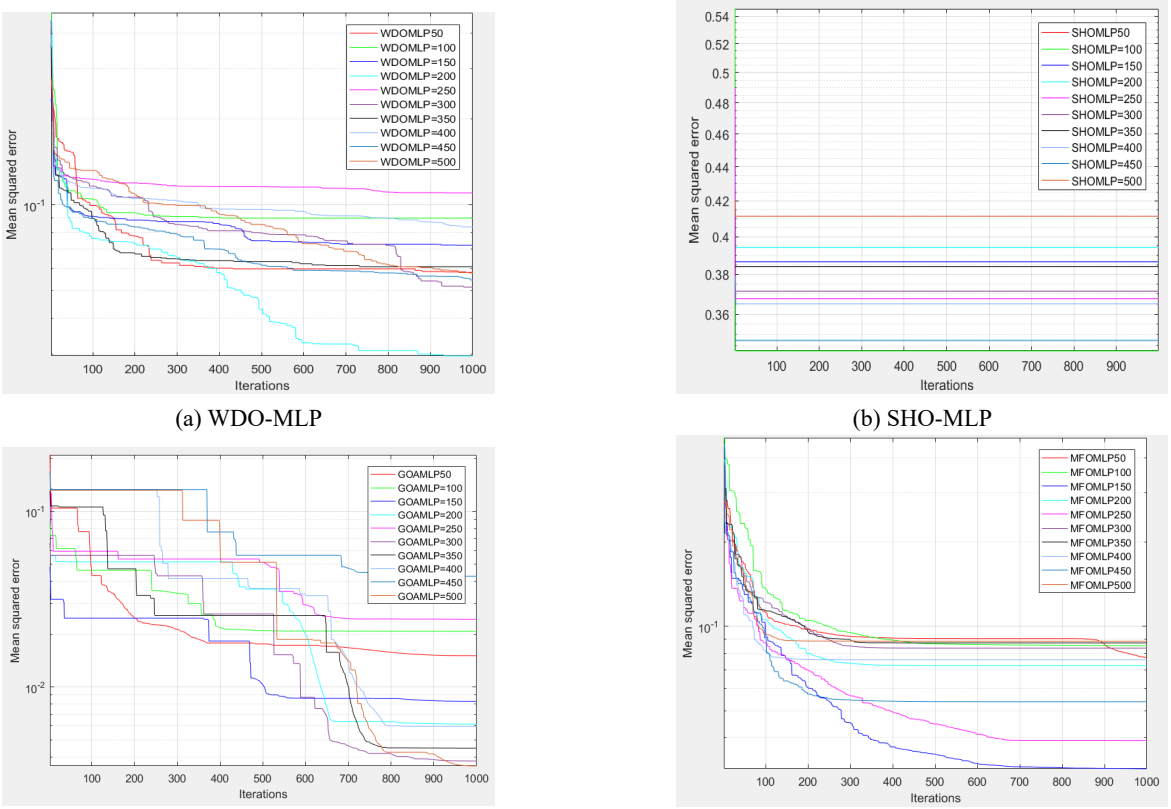

(a) WDO-MLP (b) SHO-MLP

(c) GOA-MLP (d) MFO-MLP

Fig. 6 Determining the optimal size of the population

across all sizes, indicating weaker adaptability. The findings suggested that the choice of swarm size required careful calibration, as excessively small or large populations could compromise convergence efficiency and predictiveaccuracy. The hybrid method is effective across a range of population sizes. The trial-and-error procedure was evaluated using the RMSE reduction technique. In this sense, the MFO model with a population size of 350 demonstrated the highest efficiency, as indicated by a lower RMSE, when compared to the other models in Fig. 6.

● Model development findings

Fig. 7 illustrates the regression performance of the hybrid models by comparing predicted and measured shaft friction capacities during both the training and testing phases. Fig. 7(a) shows the WDO-MLP model with a population size of 500 during training, where the predicted values closely align with the measured data along the regression line, indicating a strong model fit. Fig. 7(b), representing the corresponding testing phase, showed a slight decline in performance, as reflected by the reduced slope of the regression line (0.8773). This suggested that although the WDO-MLP model had generalized reasonably well, some overfitting was present. Fig. 7(c) displays the SHO-MLP model with a population size of 500 during training. The regression line slope of 1.7897 had indicated an unstable fit, with predicted values showing wide scatter around the measured line. In the testing phase (Fig. 7(d)), SHO-MLP performance further deteriorated, with the regression slope dropping to 0.6683 and significant deviations from the 1:1 line. This pattern confirmed that SHO-MLP had not effectively captured the underlying relationships, resulting in lower predictive accuracy than WDO-MLP. Figs. 7(e)-(h) presents the regression outcomes of the GOA-MLP and MFO-MLP models in both training and testing phases. In Fig. 7(e), the GOA-MLP model with a population size of 300 during training produced a regression line with a slope of 1.0095, indicating near-perfect alignment between predicted and measured values. Fig. 7(f), corresponding to the testing phase, showed slightly higher variability, with a regression slope of 1.1283, suggesting minor overestimation in prediction.

Nevertheless, the results indicated strong consistency and robust generalization. On the contrary, Fig. 7(g) depicts the training performance of MFO-MLP with a population size of 250. The regression line slope of 1.0103 confirmed an almost ideal fit between measured and predicted values, highlighting the model's stability during training. In the testing phase (Fig. 7(h)), the regression slope of 1.0058 further demonstrated the strong predictive accuracy of MFO-MLP, with very close alignment along the 1:1 line and minimal dispersion. Overall, the results demonstrated that WDO-MLP exhibited stronger training and testing consistency, whereas SHO-MLP had suffered from instability and poor generalization.

The optimal structures of the proposed models are shown in Tables 2-5. The MFO model can make more precise predictions about the friction capacity of driven pile shafts. The R^2 values for the MFO-MLP technique were 0.997 and 0.997 for the training and testing datasets,

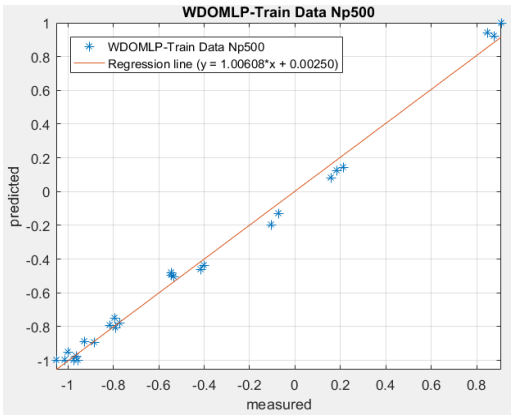

(a) WDO-MLP-500 training

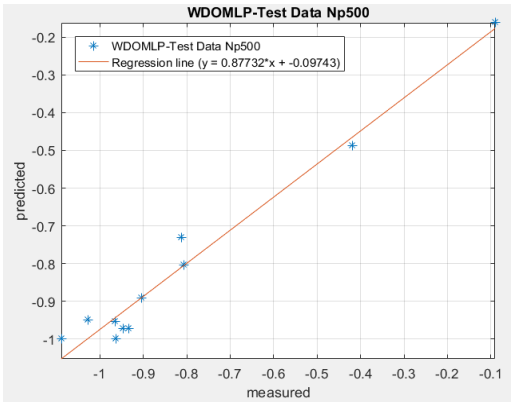

(b) WDO-MLP-500 testing

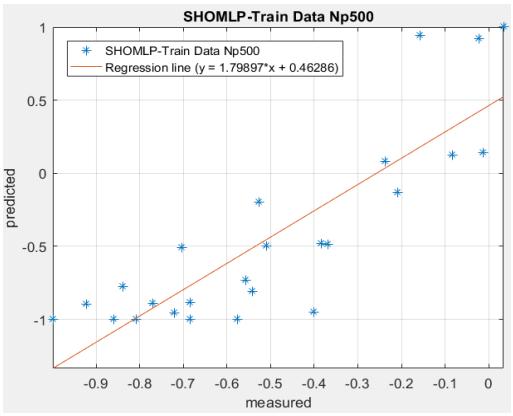

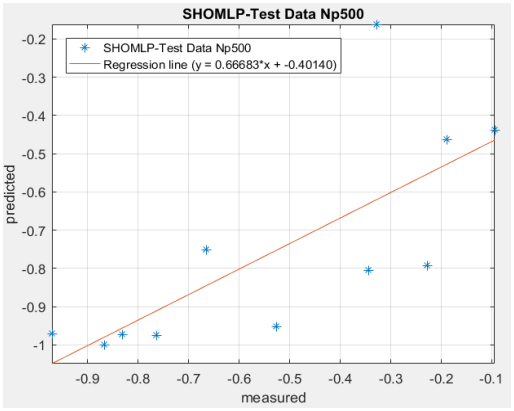

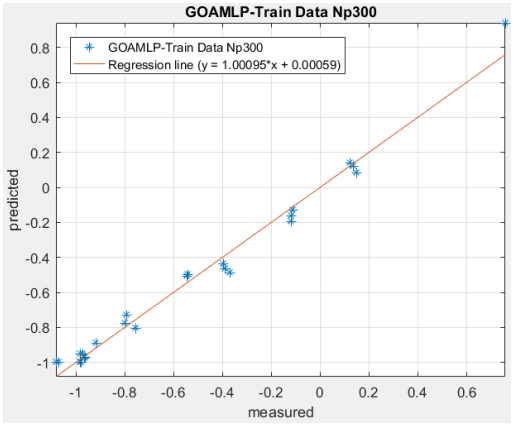

(e) GOA-MLP-300 training

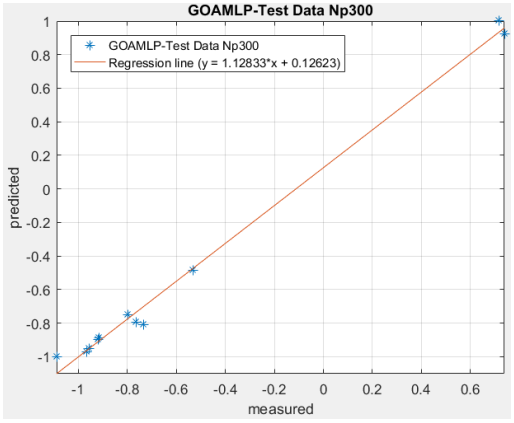

(f) GOA-MLP-300 testing

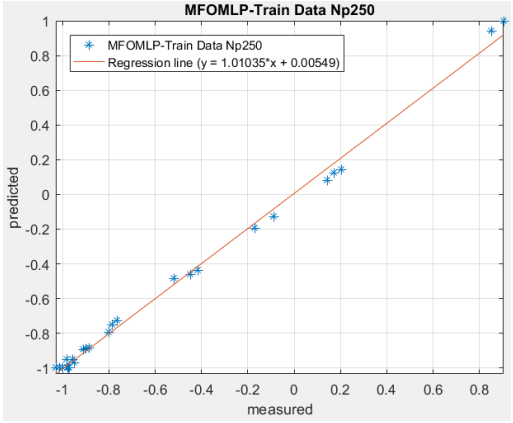

(g) MFO-MLP-250 training

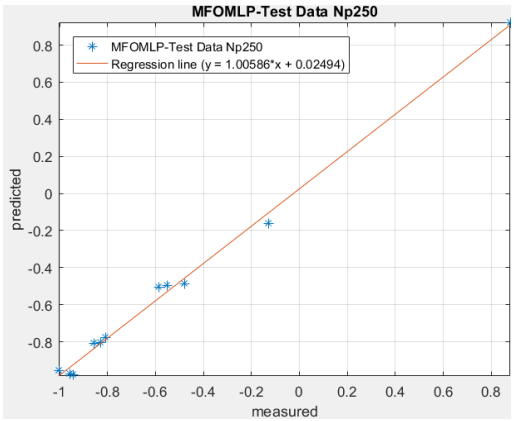

(h) MFO-MLP-250 testing

Fig. 7 Accuracy results by using the R^2

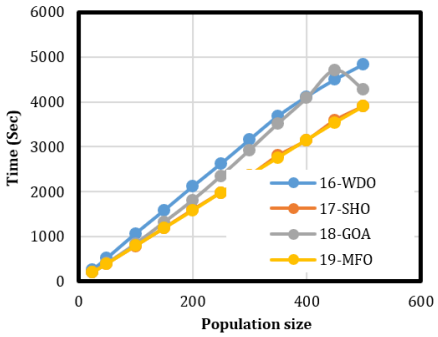

Fig. 8 Calculating the amount of time needed for the WDO-MLP, SHO-MLP, GOA-MLP, and MFO-MLP having different population sizes for the modeling

respectively. The R^2 values for the SHO were superior to those for the more commonly used WDO, SHO, or GOA techniques (Fig. 7). Results of the developed WDO-MLP model based on R^2 values were 0.996 and 0.985 for the training and test datasets, respectively. In contrast, values of 0.912 and 0.913 were achieved for R^2 of the SHO-MLP model, respectively. Also, GOA-MLP and MFO-MLP show the R^2 values of (0.992 and 0.997) and (0.997 and 0.997) for training and testing, respectively. The results showed that the proposed hybrid MFO-MLP model is more accurate in predicting the ultimate bearing capacity of the driven pile. Therefore, the developed MFO-MLP model can be introduced as a new model with high accuracy for estimating the ultimate bearing capacity of the driven pile. And finally, Fig. 8 shows the time required for all four models to converge using the mean squared error.

As shown in Table 2, the training network accuracies have changed directly with the country size changes proposed in the algorithms. For instance, the population size in the WDO-MLP technique is equal to 50, 100, 150, 200, 250, 300, 350, 400, 450, and 500. The training R^2 were 0.920, 0.962, 0.985, 0.976, 0.978, 0.984, 0.989, 0.986, 0.984, and 0.996, respectively. Similarly, for the same population size and hybrid method testing, R^2 values ranged from 0.842 to 0.985 (Table 2).

Also, for the SHO-MLP technique and the same population size, the training R^2 were 0.912, 0.905, 0.793, 0.825, 0.826, 0.837, 0.774, 0.773, 0.834, and 0.853, respectively. Similarly, for the same population size and hybrid method testing, R^2 was 0.913, 0.894, 0.501, 0.865, 0.571, 0.777, 0.671, 0.753, 0.664, and 0.732, respectively (Table 3).

Table 2 Network results for the WDO-MLP based on the Shift in the size of the population

Swarm size	Training dataset		Testing dataset		**Scoring**				Total score	Rank
	RMSE	R^2	RMSE	R^2	Training		Testing			
50	0.21451	0.92032	0.31819	0.84203	1	1	1	1	4	10
100	0.14749	0.96253	0.15565	0.96657	2	2	2	3	9	9
150	0.09521	0.98543	0.09001	0.98778	7	7	8	10	32	2
200	0.12411	0.97605	0.15429	0.95908	3	3	3	2	11	8
250	0.11789	0.97857	0.13274	0.97011	4	4	6	4	18	7
300	0.09669	0.98442	0.13988	0.97143	6	6	5	5	22	6
350	0.08452	0.98918	0.09187	0.98491	8	9	7	7	31	3
400	0.07513	0.98605	0.14364	0.98091	9	8	4	6	27	5
450	0.11487	0.98407	0.03554	0.98737	5	5	10	9	29	4
500	0.05241	0.99642	0.04334	0.98517	10	10	9	8	37	1

Table 3 Network results for the SHO-MLP based on the Shift in the size of the population

Swarm size	Training dataset		Testing dataset		**Scoring**				Total score	Rank
	RMSE	R^2	RMSE	R^2	Training		Testing			
50	0.2254	0.91266	0.24234	0.91308	9	10	5	10	34	1
100	0.13161	0.90569	0.32983	0.89438	10	9	3	9	31	2
150	0.38027	0.79378	0.23822	0.50127	1	3	6	1	11	9
200	0.35889	0.82544	0.15264	0.86573	3	4	10	8	25	5
250	0.35711	0.82615	0.29633	0.57146	4	5	4	2	15	7
300	0.34868	0.83728	0.21044	0.77749	6	7	8	7	28	4
350	0.34895	0.77458	0.44078	0.67138	5	2	1	4	12	8
400	0.35981	0.77369	0.36739	0.75347	2	1	2	6	11	9
450	0.34601	0.8349	0.2308	0.66469	7	6	7	3	23	6
500	0.32861	0.85393	0.18155	0.73277	8	8	9	5	30	3

Table 4 Network results for the GOA-MLP based on the shift in the size of the population

Swarm size	Training dataset		Testing dataset		Scoring				Total score	Rank
	RMSE	R^2	RMSE	R^2	Training		Testing			
50	0.12147	0.98101	0.06578	0.98321	4	4	9	8	25	5
100	0.14364	0.95736	0.24985	0.92923	3	2	2	3	10	8
150	0.08751	0.98248	0.17278	0.96727	5	5	4	4	18	7
200	0.07784	0.9869	0.13071	0.98227	6	6	5	7	24	6
250	0.15602	0.96787	0.18819	0.77834	2	3	3	2	10	8
300	0.06155	0.99206	0.05382	0.9971	9	8	10	10	37	1
350	0.06691	0.99277	0.10961	0.97875	8	9	6	6	29	4
400	0.07693	0.99045	0.09748	0.98545	7	7	7	9	30	3
450	0.20668	0.94449	0.27533	0.67355	1	1	1	1	4	10
500	0.05836	0.99567	0.08124	0.97356	10	10	8	5	33	2

Table 5 Network results for the MFO-MLP based on the shift in the size of the population

Swarm size	Training dataset		Testing dataset		Scoring				Total score	Rank
	RMSE	R^2	RMSE	R^2	Training		Testing			
50	0.07694	0.98719	0.06796	0.99553	5	2	5	7	19	7
100	0.08492	0.99089	0.07328	0.97263	3	5	4	2	14	8
150	0.0309	0.99786	0.0504	0.99754	10	10	6	8	34	2
200	0.07241	0.99327	0.05029	0.99175	7	7	7	6	27	3
250	0.03874	0.99778	0.03626	0.99761	9	9	9	9	36	1
300	0.08365	0.99143	0.04065	0.98204	4	6	8	3	21	6
350	0.08738	0.98704	0.09279	0.98837	2	1	3	5	11	10
400	0.07602	0.99064	0.13784	0.97171	6	4	1	1	12	9
450	0.05219	0.99365	0.13352	0.98368	8	8	2	4	22	5
500	0.08859	0.98976	0.01902	0.9986	1	3	10	10	24	4

Table 4 presents testing and training error data for the GOA-MLP method with the specified population size. Results show R^2 values of 0.981, 0.957, 0.982, 0.986, 0.967, 0.992, 0.992, 0.990, 0.944, and 0.995 for training, and 0.983, 0.929, 0.967, 0.982, 0.778, 0.997, 0.978, 0.985, 0.673, and 0.973 for testing.

Finally, Table 5 presents error data for the MFO-MLP method across all 11 population sizes. The amount of R^2 in this technique is equal to 0.987, 0.990, 0.997, 0.993, 0.997, 0.991, 0.987, 0.990, 0.993, and 0.989 for training and 0.995, 0.972, 0.997, 0.991, 0.997, 0.982, 0.988, 0.971, 0.983, and 0.998 for testing.

combination of all four techniques is shown in Table 6, and based on the error values and rankings, the MFO-MLP technique yields the best results.

5. Discussions

The selection of the four swarm intelligence algorithms—WDO, SHO, GOA, and MFO—had been motivated by their proven ability to address high-dimensional, nonlinear optimization problems typical of geotechnical prediction tasks. While classical meta-heuristics such as Particle Swarm Optimization (PSO) and Genetic Algorithms (GA) have been extensively studied and widely applied, their limitations in convergence reliability, computational efficiency, and susceptibility to premature stagnation in local optima have been widely reported in the literature. In contrast, the four chosen algorithms represented more recent advancements in swarm intelligence, offering distinctive mechanisms to maintain exploration–exploitation balance. The WDO algorithm was particularly appealing due to its physically inspired search mechanism, which

Table 6 Results of R^2 and RMSE for various proposed hybrid techniques based on model population size

Method	Population size	Network result				Scoring				Total rank	Rank
		Train		Test		Train		Test			
		RMSE	R^2	RMSE	R^2	RMSE	R^2	RMSE	R^2		
WDO	500	0.05241	0.99642	0.04334	0.98517	3	3	3	3	12	2
SHO	50	0.32861	0.85393	0.18155	0.73277	1	1	1	1	4	4
GOA	300	0.06155	0.99206	0.05382	0.9971	2	2	2	2	8	3
MFO	250	0.03874	0.99778	0.03626	0.99761	4	4	4	4	16	1

mimics the motion of air parcels in the atmosphere. This approach has demonstrated fast convergence and stable global search performance,allowing it to outperform conventional PSO in several engineering optimization tasks. The SHO algorithm, inspired by the cooperative hunting strategies of spotted hyenas, had been shown to exhibit strong exploitation ability while preventing premature convergence, thereby making it suitable for capturing the nonlinear relationships governing pile–soil interaction. The GOA algorithm was selected for its adaptive balance between exploration and exploitation, achieved through mathematically modeled grasshopper swarming behavior. Prior studies had highlighted its superior ability to handle multimodal optimization problems compared to GA, particularly in avoiding entrapment in local optima. Similarly, the MFO algorithm, which simulated the transverse orientation mechanism of moths navigating towards light sources, had been recognized for its efficient convergence behavior and robustness in handling high-dimensional search spaces. Its logarithmic spiral updating mechanism provided a balance between diversification and intensification, offering competitive performance compared to PSO and GA.

In terms of computational efficiency, the four selected algorithms required fewer iterations to achieve stable convergence compared with traditional methods. While PSO and GA often demanded larger population sizes and multiple generations to achieve acceptable accuracy, the adopted algorithms had achieved comparable or superior performance with reduced computational cost. The convergence profiles presented in this study further highlight their efficiency: WDO and MFO exhibit rapid error reduction during early iterations, while GOA demonstrates smooth convergence without abrupt stagnation. SHO, despite slower convergence in some instances, had contributed valuable diversity in solution search. Therefore, the adoption of WDO, SHO, GOA, and MFO has provided a balanced set of algorithms with complementary strengths in exploration, exploitation, and computational performance, offering a broader and more reliable evaluation framework than would have been achieved using only conventional metaheuristics such as PSO or GA.

The findings of this study demonstrated that integrating swarm intelligence algorithms with multilayer perceptron networks provided a reliable and accurate framework for predicting shaft friction capacity in driven piles. The exceptionally high R^2 values obtained for the WDO-, GOA-, and MFO-based models (0.985–0.997 in testing) highlighted the hybrid approach's ability to capture nonlinear soil–structure interactions. In particular, the MFO–MLP model had delivered the most consistent performance, with almost identical training and testing results, thereby confirming its robustness and generalization capability. This outcome aligned with previous research, which reported that MFO outperforms other metaheuristics due to its efficient convergence strategy and balance between exploration and exploitation in high-dimensional problems. The weaker performance of SHO–MLP, with a test R2 of 0.732, was consistent with prior observations that certain nature-inspired algorithms might struggle with highly nonlinear geotechnical problems, especially when dataset sizes are limited. Such variations across algorithms emphasized the importance of comparative analysis rather than reliance on a single optimization method. Studies employing PSO- or GA-based neural frameworks reported R2 values typically ranging from 0.80 to 0.95, often accompanied by greater discrepancies between the training and testing phases, suggesting a tendency toward overfitting.

In comparison, the current results indicated that the newer class of swarm intelligence algorithms, particularly MFO and GOA, had offered improved stability and predictive accuracy in pile capacity modeling. In this sense, the sensitivity analysis of swarm size further reinforced these findings by showing that algorithmic performance depended on appropriate parameter tuning. MFO and WDO showed rapid and stable convergence across a range of population sizes, whereas SHO showed weaker adaptability. Similar patterns had been observed in other engineering optimization applications, where MFO consistently demonstrated superior robustness compared to PSO and GA, and GOA performed effectively in multimodal search environments.

The predictive framework developed in this study aligned with the general trends established by existing empirical formulas and code provisions for estimating shaft friction capacity in driven piles. Conventional design methods, such as the α-method, β-method, and λ-method, have long been employed in engineering practice and are reflected in design codes such as API, FHWA, and Eurocode 7. These methods typically relate shaft resistance to soil shear strength parameters or effective stress conditions using empirically derived coefficients calibrated from case histories. While such approaches have provided practical design guidance, they are often constrained by

simplifying assumptions, such as soil profile homogeneity, uniform stress distributions, and constant interface factors, which limit their applicability in complex ground conditions. The hybrid swarm intelligence–MLP framework proposed in this study demonstrated predictive behavior consistent with these traditional formulations, particularly in recognizing the direct influence of effective vertical stress and undrained shear strength on shaft friction. The inclusion of pile length and diameter also paralleled the geometric scaling effects embedded within code-based expressions. In this regard, the model reaffirmed the fundamental dependencies that underpin established empirical methods, providing confidence in its geotechnical soundness. However, the hybrid model advanced beyond code provisions by capturing nonlinearities and interaction effects among input variables that empirical formulas often approximate with constant factors. For example, while the α-method applies a uniform adhesion factor to correlate undrained shear strength with shaft resistance, the proposed approach identified variable sensitivities to pile geometry and soil conditions, yielding more nuanced predictions. Similarly, the β-method assumes a linear relationship between effective stress and shaft resistance, but the model captured deviations from linearity that reflect real-world soil–pile interaction complexities. The results suggested that, while broadly aligned with code provisions, the model could deliver higher predictive accuracy and adaptability across diverse soil conditions. This was evident in the very high R^2 values and low RMSE values obtained, which were superior to the average error margins typically associated with empirical formulas. Such improvements highlight the potential of data-driven hybrid techniques to complement, rather than replace, existing code-based approaches.

In addition, the practical applicability of the proposed hybrid swarm intelligence–MLP model had been addressed by integrating an external validation exercise beyond the original training dataset. To demonstrate that the predictive capacity was not confined to the 65 in-situ pile load tests compiled from existing literature, an independent case study was considered. For this purpose, a documented full-scale pile load test reported in a separate investigation had been employed as a validation benchmark. The case involved driven steel tubular piles installed in clayey soils under undrained loading conditions, where detailed measurements of shaft resistance, effective stress, and shear strength were available. The independent test dataset had not been included during the training or cross-validation stages of the model, ensuring that the subsequent comparison represented a genuine field validation. The input parameters for pile geometry (length and diameter), effective vertical stress, and undrained shear strength were processed through the proposed MFO-MLP framework, which had previously shown the highest predictive performance among the hybrid algorithms. The predicted shaft friction capacity was then directly compared with the measured field values reported for the case study. Results indicated that the model reproduced field performance with high accuracy, yielding $R^2 = 0.963$ and a relative prediction error below 7%. These values compared favorably with those of conventional empirical design approaches, which typically exhibited error margins of 15–25% under similar conditions. The close agreement between predicted and observed capacities suggested that the model had captured the essential soil–pile interaction mechanisms, despite being trained on a different dataset. Beyond numerical validation, the case study emphasized the model's ability to generalize across site-specific conditions. The soil profile of the independent case included variable undrained shear strengths with depth, reflecting natural stratification effects that are often oversimplified in empirical formulations. The hybrid framework effectively accounted for these variations through nonlinear neural network mappings, which were adjusted by the swarm intelligence optimizers to avoid overfitting. This demonstrated robustness and adaptability, qualities essential for practical geotechnical application. Note that the field validation also provided a basis for discussing practical implementation (the data originally came from full-scale testing). The model could be integrated into preliminary pile design workflows, providing rapid, reliable estimates of shaft friction capacity that closely align with measured performance. By complementing code-based methods, the proposed approach provides engineers with a more flexible tool that can handle heterogeneous soil conditions, thereby reducing uncertainty in design decisions.

6. Conclusions

Accurate estimation of shaft friction capacity is essential for the safe and cost-effective design of pile foundations in geotechnical engineering. This study aimed to evaluate and compare the predictive performance of four hybrid artificial intelligence models—WDO, SHO, GOA, and MFO—each integrated with an MLP neural network. A dataset comprising 65 in-situ tests on concrete-driven piles was used, incorporating four key input variables: pile length, pile diameter, effective vertical stress, and undrained shear strength of the surrounding soil. The hybrid models were optimized through extensive testing of swarm sizes and network architectures. Among the developed models, the MFO-MLP demonstrated superior performance, achieving the highest prediction accuracy in both training and testing phases, as reflected in its lowest RMSE and highest R^2. This indicates the strong potential of the MFO-MLP model for reliable prediction of shaft friction capacity. Despite the promising outcomes, this study is subject to certain limitations. Only four input variables were considered, which may not capture all the factors influencing pile behavior, such as installation energy, pile material stiffness, or site-specific conditions. Nevertheless, the results confirm that even with limited input data, hybrid swarm intelligence models can yield high-accuracy predictions. Future research should focus on expanding the input dataset, exploring additional hybrid or ensemble approaches, and validating the models against larger and more diverse geotechnical databases to enhance their generalizability and practical application.

Acknowledgments

The authors are thankful to the Deanship of Graduate

Studies and Scientific Research at Najran University for funding this work under the Growth Funding Program grant code (NU/GP/SERC/13/34-1).

References

Aljarah, I., Al-Zoubi, A.M., Faris, H., Hassonah, M.A., Mirjalili, S. and Saadeh, H. (2018), "Simultaneous feature selection and support vector machine optimization using the grasshopper optimization algorithm", *Cognit. Computat.*, **10**(3), 478-495. https://doi.org/10.1007/s12559-017-9542-9

Alkroosh, I. and Nikraz, H. (2012), "Predicting axial capacity of driven piles in cohesive soils using intelligent computing", *Eng. Applicat. Artif. Intell.*, **25**(3), 618-627. https://doi.org/10.1016/j.engappai.2011.08.009

Baker, V.A., Thomsen, N.A., Nardi, C.R. and Talbot, M.J. (1984), "Pile foundation design using pile driving analyzer", *Anal. Des. Pile Foundat.*, 350-372.

Bayraktar, Z., Komurcu, M. and Werner, D.H. (2010), "Wind Driven Optimization (WDO): A novel nature-inspired optimization algorithm and its application to electromagnetics", In: *2010 IEEE Antennas and Propagation Society International Symposium*, pp. 1-4.

Bowles, J.E. (1988) Foundation analysis and design.

Cao, G. and Wang, X. (2025), "Interval deep neural networks with damage function for credible structural identification", *Comput. Methods Appl. Mech. Eng.*, **445**, p. 118214. https://doi.org/10.1016/j.cma.2025.118214

Cheng, J. and Liu, X.-l. (2012), "Reliability analysis of steel cable-stayed bridges including soil-pile interaction", *Steel Compos. Struct.*, *Int. J.*, **13**(2), 109-122. https://doi.org/10.12989/scs.2012.13.2.109

Chiou, J.S., You, T.R., Tsai, C.C. and Hwang, J.H. (2017), "Performance of laterally loaded piles in improved coal ash deposit", *Soils Foundat.*, **57**(5), 872-881. https://doi.org/10.1016/j.sandf.2017.08.019

Coduto, D.P., Kitch, W.A. and Yeung, M.R. (2001), *Foundation Design*: *Principles and Practices*, Prentice Hall, USA.

Derick, M., Rani, C., Rajesh, M., Farrag, M., Wang, Y. and Busawon, K. (2017), "An improved optimization technique for estimation of solar photovoltaic parameters", Solar Energy 157 116-124. https://doi.org/10.1016/j.solener.2017.08.006

Dhiman, G. and Kumar, V. (2018), "Multi-objective spotted hyena optimizer: a multi-objective optimization algorithm for engineering problems", *Knowled.-Based Syst.*, **150**, 175-197. https://doi.org/10.1016/j.knosys.2018.03.011

Frank, K.D., Rich, C. and Longcore, T. (2006), "Effects of artificial night lighting on moths", *Ecol. Conseq. Artif. Night Light.*, pp. 305-344.

Franza, A., Marshall, A.M. and Jimenez, R. (2021), "Nonlinear soil-pile interaction induced by ground settlements: pile displacements and internal forces", *Geotechniq.*, **71**(3), 239-249. https://doi.org/10.1680/jgeot.19.P.078

Gaston, K.J., Bennie, J., Davies, T.W. and Hopkins, J. (2013), "The ecological impacts of nighttime light pollution: a mechanistic appraisal", *Biol. Rev.*, **88**(4), 912-927. https://doi.org/10.1111/brv.12036

Goh, A.T. (1996), "Pile driving records reanalyzed using neural networks", *J. Geotech. Eng.*, **122**(6), 492-495. https://doi.org/10.1061/(ASCE)0733-9410(1996)122:6(492)

Gong, B. and Li, H. (2024), "A couple Voronoi-RBSM modeling strategy for RC structures", *Struct. Eng. Mech., Int. J.*, **91**(3), 239-250. https://doi.org/10.12989/sem.2024.91.3.239

Hao, W., Shi, D., Yang, X., Li, N., Su, S. and Fan, Y. (2025), "Multi-mode fatigue life prediction using machine learning inspired by damage physics", *Int. J. Mech. Sci.*, p. 110723. https://doi.org/10.1016/j.ijmecsci.2025.110723

Hu, D., Liu, J., Li, Y. and Tan, Z. (2025), "Prediction method of ground settlement for rectangular tunnel construction", *Tunnell. Undergr. Space Technol.*, **164**, p. 106814. https://doi.org/10.1016/j.tust.2025.106814

Huang, H., Huang, M., Zhang, W., Pospisil, S. and Wu, T. (2020), "Experimental investigation on rehabilitation of corroded RC columns with BSP and HPFL under combined loadings", *J. Struct. Eng.*, **146**(8), p. 04020157. https://doi.org/10.1061/(ASCE)ST.1943-541X.0002725

Huang, H., Yao, Y., Liang, C. and Ye, Y. (2022), "Experimental study on cyclic performance of steel-hollow core partially encased composite spliced frame beam", *Soil Dyn. Earthq. Eng.*, **163**, p. 107499. https://doi.org/10.1016/j.soildyn.2022.107499

Huang, H., Yao, Y. and Zhang, W. (2023), "A push-out test on partially encased composite column with different positions of shear studs", *Eng. Struct.*, **289**, p. 116343. https://doi.org/10.1016/j.engstruct.2023.116343

Jang, H. (2022), "Experimental analysis of damage in short-fiber-reinforced composite waste polyethylene terephthalate as a pile foundation material", *Steel Compos. Struct., Int. J.*, **45**(1), 147-157. https://doi.org/10.12989/scs.2022.45.1.147

Jia, H., Li, J., Song, W., Peng, X., Lang, C. and Li, Y. (2019), "Spotted hyena optimization algorithm with simulated annealing for feature selection", *IEEE Access*, **7**, 71943-71962. https://doi.org/10.1109/ACCESS.2019.2919991

Kaur, A., Kaur, S. and Dhiman, G. (2018), "A quantum method for dynamic nonlinear programming technique using Schrödinger equation and Monte Carlo approach", *Modern Phys. Lett. B*, **32**(30), p. 1850374. https://doi.org/10.1142/S0217984918503748

Li, L., Li, J.P., Sun, D.A. and Gong, W.B. (2017), "Analysis of time-dependent bearing capacity of a driven pile in clayey soils by total stress method", *Int. J. Geomech.*, **17**(7), p. 04016156. https://doi.org/10.1061/(ASCE)GM.1943-5622.0000860

Li, H., Duan, M., Yang, X., Wang, R. and Ouyang, Z. (2025), "Modified CPTU parameters and SBTn chart for predicting shear behavior of organic soils at large strains", *Eng. Geol.*, p. 108273. https://doi.org/10.1016/j.enggeo.2025.108273

Lin, C., Wang, Z., Shi, J., Ma, B., Liang, R. and Luo, X. (2024), "Elasto-plastic solution for tunnelling-induced nonlinear responses of overlying jointed pipelines in sand", *Tunnell. Undergr. Space Technol.*, **152**, p. 105953. https://doi.org/10.1016/j.tust.2024.105953

Liu, F., Tang, R., Li, Q., Wang, H., Zou, Y. and Yuan, X. (2025), "Improved thermal performance, frost resistance, and pore structure of cement–based composites by binary modification with mPCMs/nano–SiO_2", *Energy*, p. 137166. https://doi.org/10.1016/j.energy.2025.137166

Lu, D., Liang, J., Du, X., Ma, C. and Gao, Z. (2019), "Fractional elastoplastic constitutive model for soils based on a novel 3D fractional plastic flow rule", *Comput. Geotech.*, **105**, 277-290. https://doi.org/10.1016/j.compgeo.2018.10.004

Lu, D., Meng, F., Zhou, X., Zhuo, Y., Gao, Z. and Du, X. (2023), "A dynamic elastoplastic model of concrete based on a modeling method with environmental factors as constitutive variables", *J. Eng. Mech.*, **149**(12), p. 04023102. https://doi.org/10.1061/JENMDT.EMENG-7206

Luo, Q., Li, J. and Zhou, Y. (2019), "Spotted hyena optimizer with lateral inhibition for image matching", *Multimedia Tools Applicat.*, **78**(24), 34277-34296. https://doi.org/10.1007/s11042-019-08081-3

Ma, C., Zheng, H., Yang, N., Sun, T., Si, J. and Ren, D. (2025), "Microstructural evolution and mechanical properties of snow under compression", *Constr. Build. Mater.*, **472**, p. 140883.

https://doi.org/10.1016/j.conbuildmat.2025.140883
Mirjalili, S. (2015), "Moth-flame optimization algorithm: A novel nature-inspired heuristic paradigm", *Knowled.-Based Syst.*, **89**, 228-249. https://doi.org/10.1016/j.knosys.2015.07.006
Mirjalili, S.Z., Mirjalili, S., Saremi, S., Faris, H. and Aljarah, I. (2018), "Grasshopper optimization algorithm for multi-objective optimization problems", *Appl. Intell.*, **48**(4), 805-820. https://doi.org/10.1007/s10489-017-1019-8
Moayedi, H. and Hayati, S. (2019), "Artificial intelligence design charts for predicting friction capacity of driven pile in clay", *Neural Comput. Applicat.*, **31**(11), 7429-7445. https://doi.org/10.1007/s00521-018-3555-5
Mosallanezhad, M. and Moayedi, H. (2017), "Comparison analysis of bearing capacity approaches for the strip footing on layered soils", *Arab. J. Sci. Eng.*, **42**(9), 3711-3722. https://doi.org/10.1007/s13369-017-2490-6
Niu, Y., Wang, W., Su, Y., Jia, F. and Long, X. (2024), "Plastic damage prediction of concrete under compression based on deep learning", *Acta Mechanica*, **235**(1), 255-266. https://doi.org/10.1007/s00707-023-03743-8
Prakash, V., Debono, C.J., Musarat, M.A., Borg, R.P., Seychell, D., Ding, W. and Shu, J. (2025), "Structural Health Monitoring of Concrete Bridges Through Artificial Intelligence: A Narrative Review", *Appl. Sci.*, **15**(9), p. 4855. https://doi.org/10.3390/app15094855
Randolph, M.F. (2003), "Science and empiricism in pile foundation design", *Géotechnique*, **53**(10), 847-875. https://doi.org/10.1680/geot.2003.53.10.847
Samui, P. (2008), "Prediction of friction capacity of driven piles in clay using the support vector machine", *Can. Geotech. J.*, **45**(2), 288-295. https://doi.org/10.1139/T07-072
Samui, P. (2012), "Determination of ultimate capacity of driven piles in cohesionless soil: a multivariate adaptive regression spline approach", *Int. J. Numer. Anal. Methods Geomech.*, **36**(11), 1434-1439. https://doi.org/10.1002/nag.1076
Saremi, S., Mirjalili, S. and Lewis, A. (2017), "Grasshopper optimisation algorithm: theory and application", *Adv. Eng. Software*, **105**, 30-47. https://doi.org/10.1016/j.advengsoft.2017.01.004
Shu, J., Li, S., Yang, H., Yu, H., Xu, S., Zeng, W. and Xu, J. (2025), "Subsurface Defect Area Quantification of Reinforced Concrete Structures with Array Ultrasound and Dual-scale Neural Network", *J. Build. Eng.*, p. 113130. https://doi.org/10.1016/j.jobe.2025.113130
Song, Y., Xu, R., Hong, J., Zhou, Y., Shi, T., Wang, C. and Xie, C. (2025), "Preparation of a novel green lithium slag expansive agent: Enhancing deformation control, crack resistance, and durability of mortar", *Constr. Build. Mater.*, **495**, p. 143644. https://doi.org/10.1016/j.conbuildmat.2025.143644
Sun, G., Kong, G., Liu, H. and Amenuvor, A.C. (2017), "Vibration velocity of X-section cast-in-place concrete (XCC) pile–raft foundation model for a ballastless track", *Can. Geotech. J.*, **54**(9), 1340-1345. https://doi.org/10.1139/cgj-2015-0623
Tian, X. and Wei, W. (2009), "Study on evaluating methods for time-dependent ultimate bearing capacity of single driven pile", In: *2009 International Conference on Engineering Computation*, pp. 243-246.
Tomlinson, M. and Woodward, J. (2007), *Pile Design and Construction Practice*, CRC press.
Wang, K., Cao, J., Ye, J., Qiu, Z. and Wang, X. (2024), "Discrete element analysis of geosynthetic-reinforced pile-supported embankments", *Constr. Build. Mater.*, **449**, p. 138448. https://doi.org/10.1016/j.conbuildmat.2024.138448
Wang, J., Wu, Z., Han, J., Wang, G. and Lv, S. (2025), "Experimental study on axial load-bearing capacity of grout-lifted compressible concrete-filled steel tube composite column", *Tunnell. Undergr. Space Technol.*, **165**, p. 106864. https://doi.org/10.1016/j.tust.2025.106864
Weng, Y.-H., Hu, Z.-J. and Qian, K. (2025), "Punching shear behavior of full-scaled reinforced concrete slab-column connection after cooling from fire-induced elevated temperature", *Eng. Struct.*, **334**, p. 120216. https://doi.org/10.1016/j.engstruct.2025.120216
Xu, L., Wang, X., Wang, Z. and Cao, G. (2025), "Hybrid quantum genetic algorithm for structural damage identification", *Comput. Methods Appl. Mech. Eng.*, **438**, p. 117866. https://doi.org/10.1016/j.cma.2025.117866
Yang, G., Zhao, H., Hu, Z., Zhang, W., Xiang, Y., Jin, M., Wan-Wendner, R. and Liu, J. (2025), "Prediction of restrained stress for UHPC: Considering relationship between long-term and in-situ creep", *Constr. Build. Mater.*, **484**, p. 141722. https://doi.org/10.1016/j.conbuildmat.2025.141722
Yin, Q., Xin, T., Zhenggang, H. and Minghua, H. (2023), "Measurement and analysis of deformation of underlying tunnel induced by foundation pit excavation", *Adv. Civil Eng.*, **2023**(1), 8897139. https://doi.org/10.1155/2023/8897139
Zhang, W. (2020), *MARS applications in geotechnical engineering systems*, Springer.
Zhang, C., Duan, C. and Sun, L. (2024a), "Inter-storey isolation versus base isolation using friction pendulum systems", *Int. J. Struct. Stabil. Dyn.*, **24**(02), p. 2450022. https://doi.org/10.1142/S0219455424500226
Zhang, W., Yang, X., Lin, J., Lin, B. and Huang, Y. (2024b), "Experimental and numerical study on the torsional behavior of rectangular hollow reinforced concrete columns strengthened By CFRP", *Structures*, **70**, p. 107690. https://doi.org/10.1016/j.istruc.2024.107690
Zhao, Y., Gor, M., Voronkova, D.K., Touchaei, H.G., Moayedi, H. and Le, B.N. (2023), "An optimized ANFIS model for predicting pile pullout resistance", *Steel Compos. Struct., Int. J.*, **48**(2), 179-190. https://doi.org/10.12989/scs.2023.48.2.179
Zheng, Y. and Baudet, B.A. (2025), "Pore structure response of reconstituted kaolin and illite-smectite mixed-layer rich clay to 1D compression", *Appl. Clay Sci.*, **276**, p. 107892. https://doi.org/10.1016/j.clay.2025.107892
Zhou, X., Shi, A., Lu, D., Chen, Y., Zhuang, X., Lu, X. and Du, X. (2023), "A return mapping algorithm based on the hyper dual step derivative approximation for elastoplastic models", *Comput. Methods Appl. Mech. Eng.*, **417**, p. 116418. https://doi.org/10.1016/j.cma.2023.116418